MAX-PLANCK-INSTITUT FÜR PLASMAPHYSIK

GARCHING BEI MÜNCHEN

Hysteresis and Onset of Chaos in Periodically Driven Nonlinear Drift Waves

He Kaifen*, A. Salat

IPP 6/275 April 1988

* Permanent address: Institute of Low Energy Nuclear Physics

Beijing Normal University

Beijing, China

Die nachstehende Arbeit wurde im Rahmen des Vertrages zwischen dem Max-Planck-Institut für Plasmaphysik und der Europäischen Atomgemeinschaft über die Zusammenarbeit auf dem Gebiete der Plasmaphysik durchgeführt.

Abstract

The driven/damped nonlinear drift equation $\partial\phi/\partial t + a\partial^3\phi/\partial t\partial^2 y + c\partial\phi/\partial y + f\phi\partial\phi/\partial y = -\epsilon\sin(Ky - \Omega t) - \gamma\phi$ is solved numerically. In (ϵ, Ω) space the properties of the solutions repeat in a selfsimilar way in cells of decreasing size for $\Omega \to 0$. Within each cell there are regions of constant, periodic, doubly periodic, etc. or chaotic energy $E(t)$ for $t \to \infty$. Regions of Ω with a "high" and a "low" branch solution of E also exist simultaneously, which gives rise to hysteresis for cyclically varied ϵ. Hopf bifurcations may take place on both branches. The width of the hystereses depends on the initial conditions. The space dependence of ϕ and its spectral properties are also studied.

1. Introduction

Density or temperature gradients in plasmas lead to excitation of drift waves /1/. Their frequency is typically of the order $\kappa_n c_s$, where $\kappa_n = \mathrm{d} \ln n/\mathrm{d}x$ is the inverse of the density gradient scale length and $c_s^2 = T_e/m_i$ is determined by the electron temperature T_e and ion mass m_i. In drift wave theory the waves are found to be linearly unstable or damped depending on the wave number vector $\mathbf{k}$, the shear of the magnetic field and the details of the plasma properties /2/, /3/. Experimental observation /4/ in fusion plasmas reveals the presence of density fluctuations with a broad peak around the drift wave frequency and a broad peak also in the wave number spectrum with $k_\perp$ perpendicular to the magnetic field in the range $k_\perp \rho_s \lesssim 1$, indicating strong nonlinear interaction of modes. Here $\rho_s = c_s/\Omega_i$, and $\Omega_i = eB/m_i c$ is the ion gyrofrequency.

It has long been realized /5/ that the inclusion of nonlinear terms leads to Korteweg-deVries (KdV) type equations with soliton-like behaviour. Meiss and Horton /6/ tried to understand observed drift wave spectra in terms of a gas of such (almost) noninteracting one-dimensional solitons propagating in the y-direction perpendicularly to the density gradient and the magnetic field $\mathbf{B} = B\hat{\mathbf{z}}$. The opposite approach was taken by Hasegawa and Mima /7/ and others /8/. They consider the turbulence resulting from the nonlinear interaction of, in principle, infinitely many modes with k_x and k_y being of the same order. A system of three nonlinearly interacting drift waves was investigated in /9/ and /10/. Chaotic behaviour may result from the deterministic system.

Here, we also explore the onset of chaos in drift waves and the existence and properties of nonchaotic solutions, but the aspects emphasized are different to those in the work above. We consider solutions regular and chaotic not only with respect to the time dependence but also with regard to space. In plasma physics work along these lines has been done mainly for Langmuir turbulence using nonlinear Schrödinger type equations. For an overview of nonlinear equations in plasma physics see, for example, /11/. Some

analytic properties of the nonlinear drift wave equation are also given there.

Our main aim in the present paper, however, is to understand the reaction of a plasma with drift waves to an external perturbing force. As a simple example we use a driving term which is periodic in space and time. Apart from the obvious case of an externally applied electromagnetic wave, the driving term might represent a simple approximation to internal modes originating from effects not explicitly included in the equation. A damping term models the absorption of energy imparted by the external forces. Since KdV type equations are so ubiquitous in physics our model equation might also be relevant in other contexts.

We consider here the equation

$$\frac{\partial \phi}{\partial t} + a\frac{\partial^3 \phi}{\partial t \partial^2 y} + c\frac{\partial \phi}{\partial y} + f\phi\frac{\partial \phi}{\partial y} = -\epsilon \sin(Ky - \Omega t) - \gamma\phi \,. \qquad (1)$$

In Sec. 2 we give a short derivation of this equation and discuss our numerical method of solution. In Sec. 3 a global overview in $(\epsilon,\ \Omega)$ space is given of the system's reaction to the driving term. The properties are found to repeat more or less in "cells" of decreasing size for $\Omega \to 0$. The energy is a useful means of classifying the long-time behaviour. It can be steady state, periodic, doubly periodic or more complicated up to chaotic. It also turns out that the system can exist in two different states of energy (the "high" and the "low" branch) for the very same external forces. The concomitant hysteresis is explored in Sec. 4 together with the Hopf bifurcations from steady state to periodic state. The steady-state potentials are presented in Sec. 5. They are found to be running waves with the same speed as the driving term.

The choice of the initial conditions does not have an effect on the two coexisting branches. It can, however, affect the place where the transition between them takes place, i.e. the width of the hysteresis (see Sec. 6).

Since the driven system has a rich variety of phenomena even before chaos sets in, we have not yet explored in detail the transition to the chaotic state. In the cases

that we present chaotic or nonchaotic behaviour in *time* is connected with the same behaviour in *space*. This need not always be the case, as results from other driven nonlinear equations suggest /12/. Also, we report here on wave numbers of the driving term $K \neq 0$ only (in fact $K = 1$). Preliminary studies with $K = 0$ have shown that the system may react differently. Further investigations are required for these topics.

2. Model equation and numerical method

Closely following the discussion in Ref. /6/, we assume the magnetic field to be constant, $\mathbf{B} = B\hat{\mathbf{z}}$, and the mean density n and electron temperature T_e to depend on the radial coordinate x only. The electron density is adiabatic:

$$n_e(\mathbf{r},t) \;=\; n(x)\,\exp[\; e\Phi(\mathbf{r},t)/T_e(x)\;]\;. \tag{2}$$

The ion fluid is pressureless and is governed by the equation of continuity

$$\frac{\partial n_i}{\partial t} \;+\nabla\cdot(n_i\mathbf{v}) \;=\; 0\;, \tag{3}$$

where $\mathbf{v} = v_{\|}\hat{\mathbf{z}} + \mathbf{v}_{\perp}$. In the drift frequency regime, $\omega << \Omega_i$, one has approximately $\mathbf{v}_{\perp} = \mathbf{v}_E + \mathbf{v}_P$, where the $\mathbf{E}\times\mathbf{B}$ drift and the polarization drift are given by, respectively,

$$\mathbf{v}_E \;=\; \frac{\hat{\mathbf{z}}\times\nabla\Phi}{B}\;, \tag{4}$$

$$\mathbf{v}_P \;=\; \frac{-1}{B\Omega_i}\left(\frac{\partial}{\partial t} \;+\; \mathbf{v}\cdot\nabla\right)\,\nabla\Phi\;, \tag{5}$$

with $\mathbf{E} = -\nabla\Phi$. The quasineutrality condition is $n_i = n_e$. As in /6/, /7/, we neglect parallel propagation, putting $\partial/\partial z = 0$. Also, we consider the one-dimensional limit $k_x(k_y\rho_s)^2 << \kappa_T$ /6/. As a result one obtains for $\phi = e\Phi/T_e$

$$\left(1 \;-\; \rho_s^2\frac{\partial^2}{\partial y^2}\right)\;\frac{\partial\phi}{\partial t} \;-\; \kappa_n c_s\rho_s\;\frac{\partial\phi}{\partial y} \;+\; \kappa_T c_s\rho_s\;\phi\frac{\partial\phi}{\partial y} \;=\; 0\;, \tag{6}$$

where $\kappa_n = (\mathrm{d}n/\mathrm{d}x)/n$ and $\kappa_T = (\mathrm{d}T_e/\mathrm{d}x)/T_e$. The term $\partial^3_{tyy}\phi$ originates from $n_i\mathrm{div}\;\mathbf{v}_{P0}$, the dispersive term from $\mathbf{v}_E\cdot\nabla n$ and the nonlinear term from $\mathbf{v}_E\cdot\nabla\tilde{n}$, where $\mathbf{v}_{P0}$ is the nonconvective part of $\mathbf{v}_P$ and $\tilde{n}$ corresponds to the Boltzmann factor in n_e. In keeping with the model character of our investigation we omit further nonlinearities which contain higher-order derivatives of ϕ and arise from the remaining combinations of the terms in $\mathbf{v}$ and n_i, in conformity with /6/, /10/ and /13/. In contrast to the 2-d turbulence scaling $k_x \approx k_y$ /7/, /8/, these terms are not dominant here.

To equation (6) we introduce *ad hoc* a periodic driving term with amplitude ϵ, wave number K and frequency Ω and a linear damping term. This yields eq. (1) with $a = -\rho_s^2$, $c = -\kappa_n c_s \rho_s$ and $f = \kappa_T c_s \rho_s$.

For toroidal plasma configurations y corresponds to a periodic poloidal coordinate. Without loss of generality we assume a periodicity interval 2π and make the spectral ansatz for $\phi(y,t)$:

$$\phi(y,t) = \sum_{k=0}^{N-1} \phi_k(t) \exp(\, iky \,) \qquad \text{at} \quad y = y_j = \frac{2\pi j}{N}, \quad j = 0, \ldots N-1. \quad (7)$$

The nonlinear term is evaluated in coordinate space with N grid points by using fast Fourier transform with dealiasing. For nonchaotic solutions $N = 128$ is often sufficient. Time integration of the ordinary differential equations for $\mathrm{d}\phi_k/\mathrm{d}t$ is performed with a standard predictor-corrector scheme with time step $\Delta t = 10^{-2}$ in most runs. To confirm chaotic evolution, it is usually necessary to run up to $t \approx 10^4$.

3. Global results on wave energy and potential

We take the applied frequency Ω and amplitude ϵ as two control parameters in our numerical experiment. The other parameters are kept fixed and are chosen arbitrarily (except for a): $a = -0.28711$, $c = 1.0$, $f = -6.0$, $\gamma = 0.1$, $K = 1$. A negative a is not only dictated by the physics but is also necessary for numerical stability of the drift wave equation (in contrast to the KdV equation). In the present paper, if not otherwise stated, we always start computation at $t = 0$ from a solitary-wave-type solution /6/ of unperturbed eq. (1) (namely, $\epsilon = 0, \gamma = 0$),

$$\phi(y, t = 0) \;=\; \phi_a \;+\; (\phi_b - \phi_a)\, \mathrm{sn}^2(c_s y,\; k) \tag{8}$$

where sn is a Jacobian elliptic function with $c_s = \sqrt{f(\phi_c - \phi_a)/(12ua)}$, $u = c + f(\phi_a + \phi_b + \phi_c)/3$ and $k = \sqrt{(\phi_b - \phi_a)/(\phi_c - \phi_a)}$. We use $\phi_a = 0$, $\phi_b = 0.0625$, $\phi_c = 0.125$, a combination which, in order to ensure 2π-periodicity of the function (8), requires the numerical value of a quoted, for given c and f. Equation (1) is then solved numerically with periodic boundary conditions.

The behaviour of eq. (1) is explored in detail in a large region of (Ω, ϵ). In addition to the potential $\phi(y, t)$, the wave energy is also and even better suited to characterising the behaviour of the system. It is defined as

$$E(t) = \frac{1}{2\pi} \int_0^{2\pi} \frac{1}{2} \left[\phi^2(y,t) \;-\; a \left(\frac{\partial \phi(y,t)}{\partial y} \right)^2 \right] \mathrm{d}y \tag{9}$$

and is a constant of the motion for $\epsilon = \gamma = 0$. As long as the energy evolves "regularly", we find that $\phi(y, t)$ does not show any signs of chaos, either.

Different types of asymptotic behaviour for $E(t)$ are observed. Some typical results are given in Figs. 1(a)-(e). In Fig. 1(a) an asymptotically steady state of $\Delta E(t) = E(t) - E(0)$ is reached for $\Omega = 0.525$ and $\epsilon = 0.06425$ ($E(0) = 7.333 \times 10^{-4}$ in all cases). For later

purposes it is interesting to note that initially the energy remains almost stationary at a lower level and then suddenly jumps to a higher level E_s, (the subscript s denotes steady state). This behaviour is an indication of the coexistence of two distinct branches of solution, as will be discussed below in detail. Figures 1(b), (c) give two examples of singly and doubly periodic oscillations for $\Delta E(t)$, respectively. Figure 1(d) is an intermediate case, at least three frequencies being distinguishable in its spectrum. In Fig. 1(e), finally, the energy is very chaotic. In Figs. 1(b)-(e) only the stationary states are shown, the transient periods having been omitted.

In Figs. 2(a)-(e) we give the space-time evolution of the potential $\phi(y,t)$ in the stationary states corresponding to Figs. 1(a)-(e). In the constant energy case, Fig. 2(a), $\phi(y,t)$ consists of travelling waves whose velocity exactly coincides with the phase velocity Ω/K of the driving term. The dependence on y and t is smooth, with two minima and maxima per period. In the case 2(b) the waves do not propagate with constant shape but are periodically twisted, so to speak, as close inspection of Fig. 2(b) reveals. This fits together with the Fourier analysis of the energy, Fig. 3(a), and of the potential at a fixed point, Fig. 3(b). The energy spectrum consists of one sharp line at $\omega = \omega_E$, corresponding to the observed periodic behaviour of $E(t)$ with period $2\pi/\omega_E$. The potential spectrum, on the other hand, is governed by the driving frequency Ω, its harmonics, and, in addition, integer combinations of Ω and ω_E. (Note the different frequency scales in Figs. 3(a) and 3(b).)

For quasiperiodic and intermediate $E(t)$, Figs. 2(c) and 2(d), travelling waves with the same speed as the driving term are still the most evident global features. However, local features and even some sloshing back and forth become more pronounced. For chaotic energy the global character is lost. The waves split into many solitons, persisting for some time and then interacting with each other, Fig. 2(e). The Fourier spectrum $\phi(\omega)$ in this case, see Fig. 4, has a broad background.

The different possibilities, as discussed above, are collected in Fig. 5 into a general

view of the behaviour of $E(t)$ in the parameter space (Ω, ϵ). In the plot, points ($\bullet$) denote asymptotic steady states of $E(t)$, open circles ($\circ$) singly periodic cases, and crosses (x) chaotic cases, while triangles (Δ) denote transition cases between singly periodic and chaotic. They can be doubly periodic or intermediate, as in Figs. 1(c) and (d).

Figure 5 is plotted for $\Omega = 0 - 0.8$, a region where the behaviour of $E(t)$ shows a rich structure. The overview is quite crude and the distinction between intermediate and chaotic cases is somewhat arbitrary. Also, running the system for longer times might change some of the characterizations. Nevertheless, it serves to show the existence of repeating "cells" scaling down with $\Omega \to 0$, possibly in a selfsimilar manner.

Let us look at the first cell from the right, $\Omega \approx 0.4 - 0.8$. There is a ground floor of steady state $E(t)$. At the low-frequency side of the cell this floor reaches up to high values of ϵ (although it may take a very long time for E to settle down). With increasing Ω there are two big finger-like regimes, in the left part of which $E(t)$ is chaotic and in the right part of which $E(t)$ is mainly periodic. In between there is a transition region. Also shown is a bifurcation line (dashed), which will be discussed below.

Apart from some details, similar behaviour is repeated in smaller and smaller scales when Ω decreases.

We also tested cases with $\Omega = 0.8 - 2.0$. The critical value of ϵ at which the asymptotic E transits to chaos continues to increase monotonically with Ω.

In the following Sections we elaborate further on some of the bifurcation lines and on phenomena which do not show up in Fig. 5.

4. Hystereses and Hopf bifurcations

In order to illustrate the dependence of the energy $E(t)$ on ϵ, we fix Ω at $\Omega = 0.525$ as an example. In the range of $\epsilon = 0 - 0.08$, the long-time behaviour is always a steady state, E_s. If we start from initial condition (8) and increase ϵ from 0, at first E_s increases gradually as a function of ϵ, but then more and more steeply, see Fig. 6, until at a critical value ϵ_h the energy abruptly jumps to a higher level. Now, if we start the calculation not from (8) but from the resulting high-level steady state, e.g. the asymptotic state reached with $\epsilon = 0.07$ (the "high-branch" initial condition), and then decrease ϵ, we find that E_s stays at a higher level until ϵ reaches another critical value $\epsilon_l < \epsilon_h$ where E_s suddenly drops back to a lower level which is the same as that calculated directly from initial condition (8). In other words, the variation of E_s with ϵ depends on initial conditions, and the $E_s(\epsilon)$ curve is a hysteresis. The same hysteresis is also obtained /14/ with the "step-by-step" procedure: ϵ is changed in small steps and the asymptotic state of $\phi(y,t)$ for the "old" ϵ is used as initial condition for the "new" ϵ.

In Fig. 7 we give a group of curves of E_s - ϵ for Ω between 0.475 and 0.60. Hysteresis is observed from $\approx$ 0.50 to $\approx$ 0.575 (not shown), as evidenced by the vertical sections. In order not to crowd the plot too much, we left out the low-ϵ part of the high branches of the hystereses. The width of the hystereses $\epsilon_h - \epsilon_l$ reduces when Ω is decreased and finally shrinks to zero. The upper and lower branches merge. At $\Omega = 0.475$ hysteresis no longer exists.

Between $\Omega \approx 0.475$ and 0.30 no hysteresis is found. The E_s- ϵ curves are smooth. Possibly this has to do with the big zone of steaty-state energies around this region in Fig. 5.

With Ω further decreased, hysteresis appears again (see Fig. 8). From $\Omega \approx 0.2825$ to 0.2875 it shows another group of hystereses. Again, their widths decrease continuously with decreasing Ω until at $\Omega \approx 0.275$ they disappear again.

Every cell in Fig. 5 can therefore be expected to be accompanied by a group of hystereses. The observed critical values ϵ_h are plotted as two dashed lines. The continuation of these lines into the upper region of the "cells" seems to be related to the transition between the periodic and the chaotic parts. We have not yet investigated these "backbones" of the cells in any detail, but we did make a study of the "flesh", namely the Hopf bifurcations, which we shall describe in the following.

For fixed Ω, increasing ϵ further can cause a steady state of energy to bifurcate into periodic motion, as we have seen in Fig. 1(b). Such a Hopf bifurcation may occur either in the lower branch or in the upper branch. In Figs. 7 and 8 the dashed lines denote asymptotic states for which $E(t)$ is not constant any more, i.e. $E = const$ loses stability. In these cases the average of the oscillating energy is plotted as E_s. In Fig. 7 it can be seen that for $\Omega = 0.6$ a Hopf bifurcation occurs when the energy is still in the lower branch, while for $\Omega = 0.50$ - 0.57 it occurs in the upper branch.

Furthermore, a solution with steady-state energy in the upper branch may lose its stability at a critical ϵ^* which is even smaller than ϵ_h. That is, as soon as the jump takes place, it leads to oscillatory behaviour. This phenomenon can be seen in Fig. 8 for $\Omega = 0.2875$. At the transition point $\epsilon_h = 0.0665$, the energy in the upper branch is already periodic. Our investigation shows that the first Hopf bifurcation of energy in the upper branch takes place at $\epsilon^* = 0.064$, in between ϵ_h and $\epsilon_l = 0.0634$. The same thing happens for $0.549 \lesssim \Omega \lesssim 0.575$.

In the region of the biggest cell we plot all these bifurcation values ϵ_h, ϵ_l and ϵ^* in Fig. 9, which is partly an enlargement of Fig. 5. The dashed lines are ϵ_h and ϵ_l. The difference between ϵ_h and ϵ_l is the width of the corresponding hysteresis, which shrinks with decreasing Ω, as mentioned above. (We did not follow ϵ_h and ϵ_l until they merge.) For $\Omega \gtrsim 0.55$ a clear-cut ϵ_l curve emerges only with the step-by-step method. Otherwise ϵ_l depends too much on the initial conditions; see below and Sec. 6.

The solid line ϵ_h^* on the l.h.s. is the Hopf bifurcation for the upper branch. In this region of Ω the lower branch does not have a Hopf bifurcation. For higher frequencies,

however, the r.h.s. has a Hopf bifurcation ϵ_l^* which belongs to the low branch there (see Fig. 7). We note that ϵ_h^* for the upper branch crosses ϵ_h at $\Omega \approx 0.549$. That is, if starting from the lower branch ϵ is increased for $0.549 < \Omega \lesssim 0.575$, the bifurcation line ϵ_h^* is crossed before ϵ_h is reached. When $\epsilon > \epsilon_h$, the system therefore jumps to a state with nonconstant energy, periodic for Ω close to the crossing point at $\Omega = 0.549$, or, if it encounters further bifurcations in between, more complicated or even chaotic.

At present we are investigating the behaviour of the system in the region $\Omega \gtrsim 0.575$, where the bifurcation lines ϵ_l , ϵ_h , ϵ_h^* collide with or come close to ϵ_l^*.

In Fig. 10 E^* vs. ϵ^* is plotted, where E^* is the value of the energy when Hopf bifurcation appears. A pair of curves is obtained for the biggest cell, a) for the upper branch and b) for the lower branch. This tells us that different amounts of energy are needed to destabilize the two branches. Presumably, this can be attributed to the different spatial patterns of $\phi(y)$ in the two branches, which will be described in the next section. Different pairs of such lines are expected for the other cells.

We plot E_s vs. Ω in Fig. 11 for the two values ϵ, $\epsilon = 0.05$ and 0.06. The initial conditions (8) are used again. The pattern observed matches with the topological features of Fig. 5. Dashed lines denote non-steady states of energy. Comparison with Fig. 7 shows that the steep sections around the peaks correspond to the high and low branches in the hystereses, with the jump to high energy taking place at the peaks. Regions without hysteresis smoothly connect the sections with hysteresis.

5. Spatial properties of the potential

Up to now we have mainly discussed the energy. In fact, when a transition of E_s between the lower and upper branches takes place, it is accompanied by a sudden change of the spatial pattern of the potential. Here we describe it for the cases with steady-state energy. Figures 12(a), (b) give two examples for $\phi(y)$ belonging to the lower and upper branches of one hysteresis. They are typical patterns on each side of the dashed line on the right in Fig. 5. In the lower branch, Fig. 12(a), $\phi(y)$ has two dips and the second harmonic dominates in its spectrum $\phi(k)$. In the transition to the upper branch, Fig. 12(b), the third harmonic suddenly becomes strong. In Fig. 12(b) this has caused a plateau in addition to two dips. With decreasing Ω the plateau develops into a new dip.

For every cell the group of transitions at ϵ_h is accompanied by such a sudden change of the patterns of $\phi(y)$. As Ω decreases, $\phi(y)$ develops more and more dips, and their phase plots (see below) develop more and more loops. Figure 13 is an example of $\phi(y)$ for $\Omega = 0.01$.

Figure 14 gives two phase plots ϕ versus $\partial\phi/\partial y$ with the data recorded in small time intervals, for (a) steady-state energy, and (b) periodic energy. In case (a) the phase plot is a closed curve with two loops. In case (b) the loops still exist but they are blurred by the motion with the additional incommensurate period.

6. Dependence on initial conditions

The effects of the initial conditions were studied with regard to the hystereses observed: We start from $\phi(y,t=0) = A\ \sin(ny + y_0)$ and watch the transition between the two branches for this particular initial condition. In contrast to the methods described in Sec. 4, we do not switch here between different initial conditions, so that the critical value of the jump, $\epsilon = \epsilon_c$, applies to coming from above or below, and $\epsilon_l = \epsilon_h = \epsilon_c$ therefore applies.

Figure 15 gives the dependence of ϵ_c on the phase y_0, the harmonic number n and the amplitude A, for $\Omega = 0.525$. The error bars are not intrinsic but merely reflect the limited number of tests made. It is obvious that y_0, n and A can all have a strong effect. The highest and the lowest values of ϵ_c agree with the previously obtained values $\epsilon_h = 0.064$, $\epsilon_l = 0.051$ (see Fig. 6). In that sense the initial condition (8) seems to play a particular role. This is confirmed when the amplitude ϕ_b is varied, or, after y is replaced by $ny + y_0$ in eq. (8), when n and y_0 are varied. In all cases tested ϵ_h and ϵ_l (for nonchaotic initial conditions) remain unchanged. Obviously, in function space the basins of attraction to the two branches have a finite extent, with the functions (8) lying more to the "center" than the sinusoidal trial functions used above.

In any case, while the places where the jumps between the upper and the lower branches occur are found to vary, it is important to note that the branches themselves do not depend on initial conditions. That is to say, the values of the energy E and the shapes of the solution $\phi(y,t)$ along the remaining sections of the branches are unaffected by the previous history. This is found to hold even when the jump to low energy occurs from a state with chaotic $E(t)$ and $\phi(y,t)$, e.g. for Ω around 0.57, see the discussion in Sec. 4. Taking chaotic $\phi(y,t)$ at arbitrary consecutive times t as initial conditions and each time decreasing ϵ from a large value yields a continuum of values for ϵ_l, but again it is found that they lie on *one* branch of the $E(\epsilon)$ curve.

References

/ 1/ B.B. Kadomtsev, Plasma Turbulence, Academic Press, London 1965.

/ 2/ A.B. Mikhailovski in Reviews of Plasma Physics, Vol. 3, Consultants Bureau, New York 1967.

/ 3/ S.P. Hirshman and K. Molvig, Phys. Rev. Lett. 42, 648 (1979);

K. Molvig, S.P. Hirshman and J.C. Whitson, Phys. Rev. Lett. 43, 582 (1979).

/ 4/ E. Mazzucato, Phys. Rev. Lett. 48, 1828 (1982);

C.M. Surko and R.E. Slusher, Phys. Fluids 23, 2425 (1980).

/ 5/ V. Oraevskii, H. Tasso and H. Wobig, in Plasma Physics and Controlled Nuclear Fusion Research [Proc. of the 3rd International Conference, Novosibirsk 1986 (IAEA, Vienna 1969)], Vol. I, p. 671.

/ 6/ J.D. Meiss and W. Horton, Phys. Fluids 25, 1838 (1982).

/ 7/ A. Hasegawa and K. Mima, Phys. Fluids 21, 87 (1987).

/ 8/ P.W. Terry and W. Horton, Phys. Fluids 26, 106 (1983);

R.E. Waltz, Phys. Fluids 26, 169 (1983);

/ 9/ P.W. Terry and W. Horton, Phys. Fluids 25, 491 (1982).

/10/ He Kaifen and D. Biskamp, Phys. Letters A 108, 347 (1985);

D. Biskamp and He Kaifen, Phys. Fluids 28, 2172 (1985).

/11/ V.G. Makhankov, Physics Reports 35, 1 (1978).

/12/ A.R. Bishop, K. Fesser, P.S. Lomdahl *et al.*, Phys. Rev. Lett. 50, 1095 (1983).

/13/ V.I. Petviashvili, Sovj. J. Plasma Phys. 3, 150 (1977).

/14/ He Kaifen and A. Salat, Report IPP 6/274 (1988), submitted for publication.

Figure captions

Fig. 1a: Energy $\Delta E = E(t) - E(0)$ as function of time. Arbitrary units. Steady-state case;

$\epsilon = 0.06425,\ \Omega = 0.525.$

Fig. 1b: Asymptotic state of ΔE for periodic case; $\epsilon = 0.0675,\ \Omega = 0.6.$

Fig. 1c: Asymptotic state of ΔE for doubly periodic case; $\epsilon = 0.0917,\ \Omega = 0.55.$

Fig. 1d: Asymptotic state of ΔE for "intermediate" case; $\epsilon = 0.12,\ \Omega = 0.35.$

Fig. 1e: Asymptotic state of ΔE for chaotic case; $\epsilon = 0.2,\ \Omega = 0.525.$

Fig. 2a: Potential $\phi(y,t)$. Earlier time in the foreground. Parameters as in Fig. 1a.

Fig. 2b: Potential $\phi(y,t)$. Parameters as in Fig. 1b.

Fig. 2c: Potential $\phi(y,t)$. Parameters as in Fig. 1c.

Fig. 2d: Potential $\phi(y,t)$. Parameters as in Fig. 1d.

Fig. 2e: Potential $\phi(y,t)$. Parameters as in Fig. 1e.

Fig. 3a: Spectrum $E(\omega)$ of energy, corresponding to Fig. 1b.

Fig. 3b: Spectrum $\phi(\omega)$ of potential at fixed y, corresponding to Fig. 2b.

Fig. 4: Spectrum $\phi(\omega)$ of potential at fixed y, corresponding to Fig. 2e.

Fig. 5: Global view of asymptotic behaviour of energy as function of driving parameters ϵ and Ω: points ($\bullet$) denote steady states, open circles ($\circ$) singly periodic cases, crosses (x) chaotic cases, and triangles (Δ) transition cases between singly periodic and chaotic.

Fig. 6: Hysteresis curve for steady-state energy E_s as function of driving amplitude ϵ. The energy jumps into the high and the low branches at the critical values ϵ_h and ϵ_l, respectively. $\Omega = 0.525.$

Fig. 7: Group of hystereses (indicated by the vertical sections of their right wings). Dotted sections: the energy does not approach a steady state. $\Omega = 0.475 - 0.6.$

Fig. 8: Another group of hystereses. $\Omega = 0.275 - 0.3.$

Fig. 9: Critical values ϵ_h, ϵ_l, dashed, and ϵ_h^*, ϵ_l^*. For $\epsilon > \epsilon_h^*$ or $\epsilon > \epsilon_l^*$ the energy does not approach a steady state any more, in the corresponding branch.

Fig. 10: Energy E^* when Hopf bifurcation sets in. Curve a) in upper branch vs. ϵ_h^*, curve b) in lower brach vs. ϵ_l^*.

Fig. 11: Steady-state energy E_s as function of Ω. Dotted section: the energy does not approach a steady state.

Fig. 12a: Travelling-wave solution $\phi(y)$ in the low branch; $\epsilon = 0.06375$, $\Omega = 0.525$.

Fig. 12b: Travelling-wave solution $\phi(y)$ in the high branch; $\epsilon = 0.06425$, $\Omega = 0.525$.

Fig. 13: Travelling-wave solution $\phi(y)$ for small Ω; $\epsilon = 0.1$, $\Omega = 0.01$.

Fig. 14a: Phase plot ϕ vs. $\partial\phi/\partial y$ at fixed y. Constant energy case; $\epsilon = 0.06375$, $\Omega = 0.525$.

Fig. 14b: Phase plot ϕ vs. $\partial\phi/\partial y$ at fixed y. Periodic energy case; $\epsilon = 0.0675$, $\Omega = 0.6$.

Fig. 15: Dependence of ϵ_c on phase y_0, harmonic number n and amplitude A of initial condition $\phi(y, t = 0) = A\sin(ny + y_0)$. Figs. a), b) with $A = 0.125$, Figs. c), d) with $A = 0.4$; $\Omega = 0.525$.

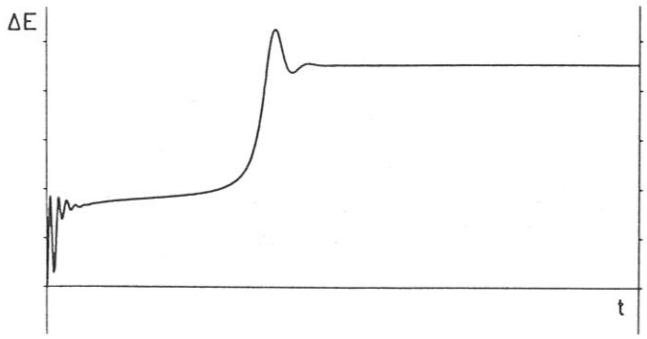

Figure 1a

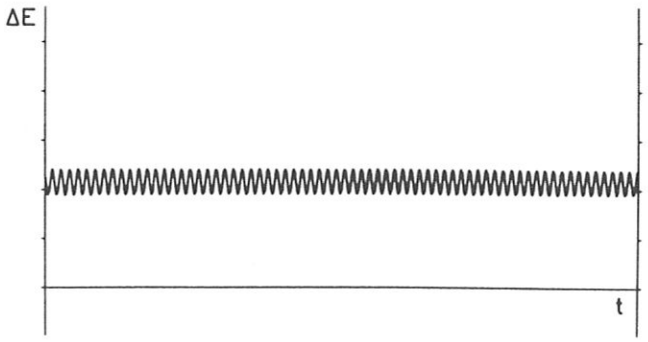

Figure 1b

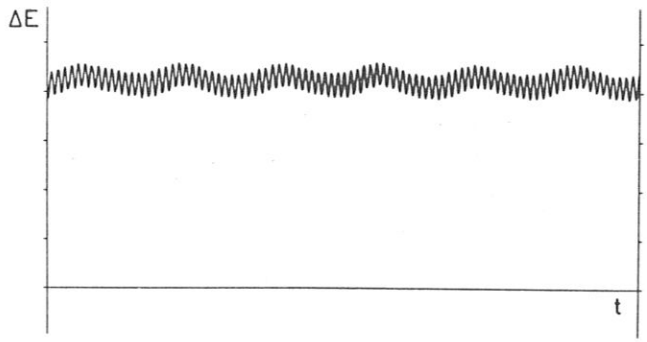

Figure 1c

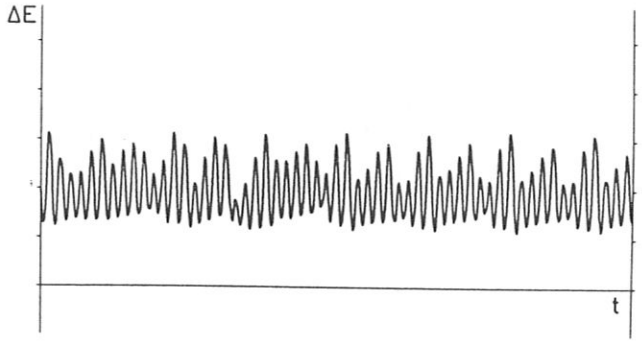

Figure 1d

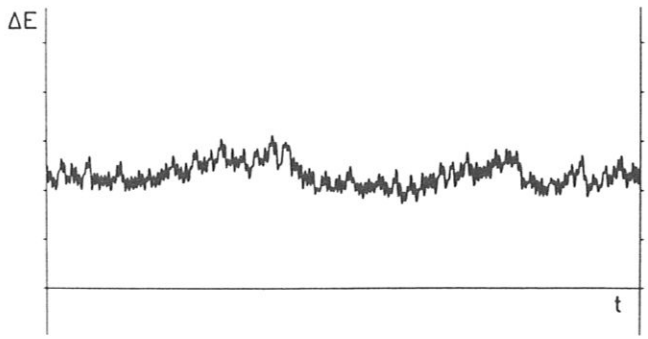

Figure 1e

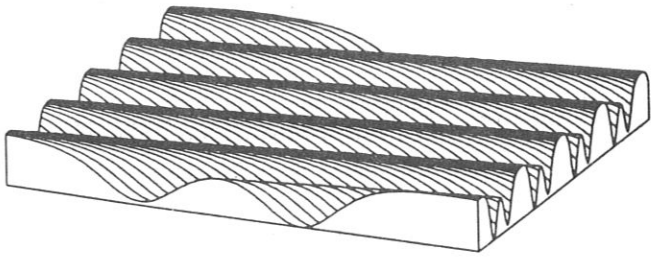

Figure 2a

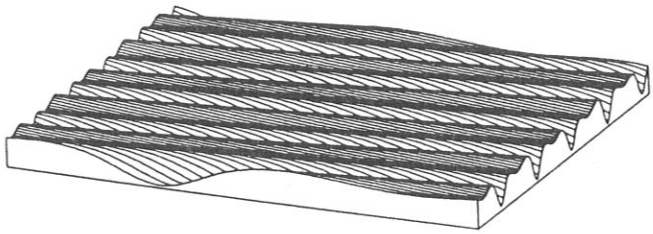

Figure 2b

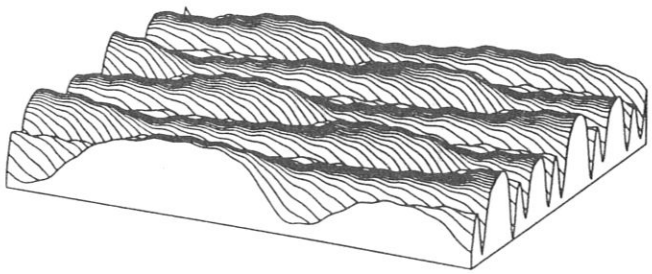

Figure 2c

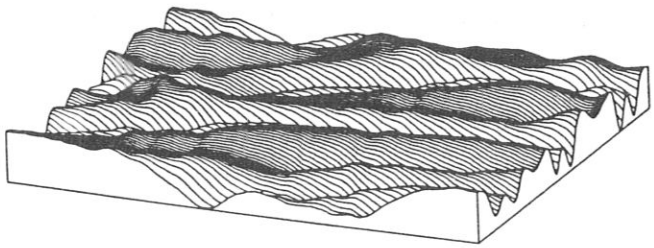

Figure 2d

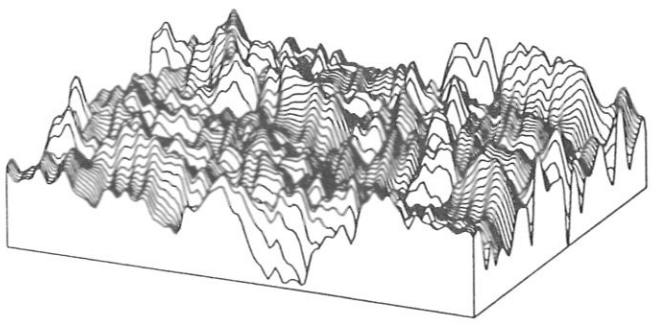

Figure 2e

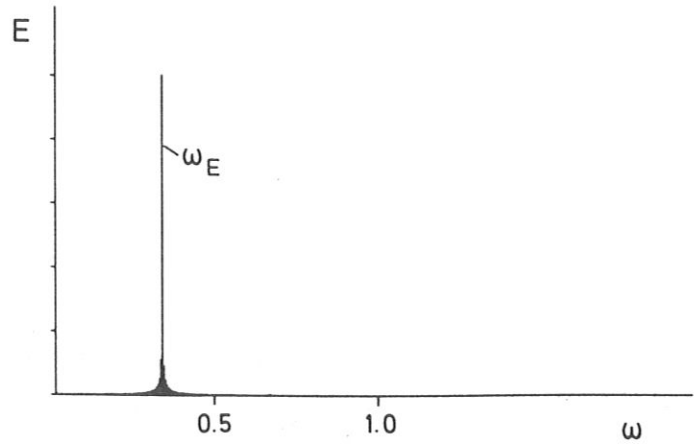

Figure 3a

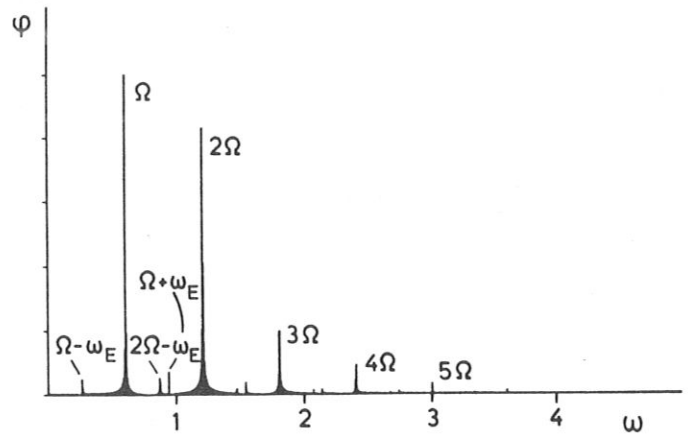

Figure 3b

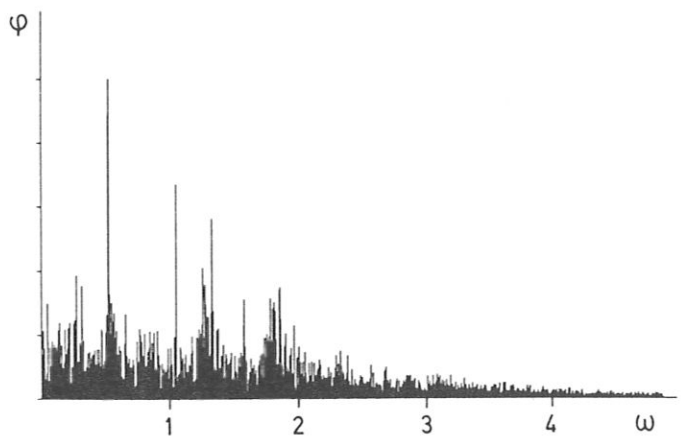

Figure 4

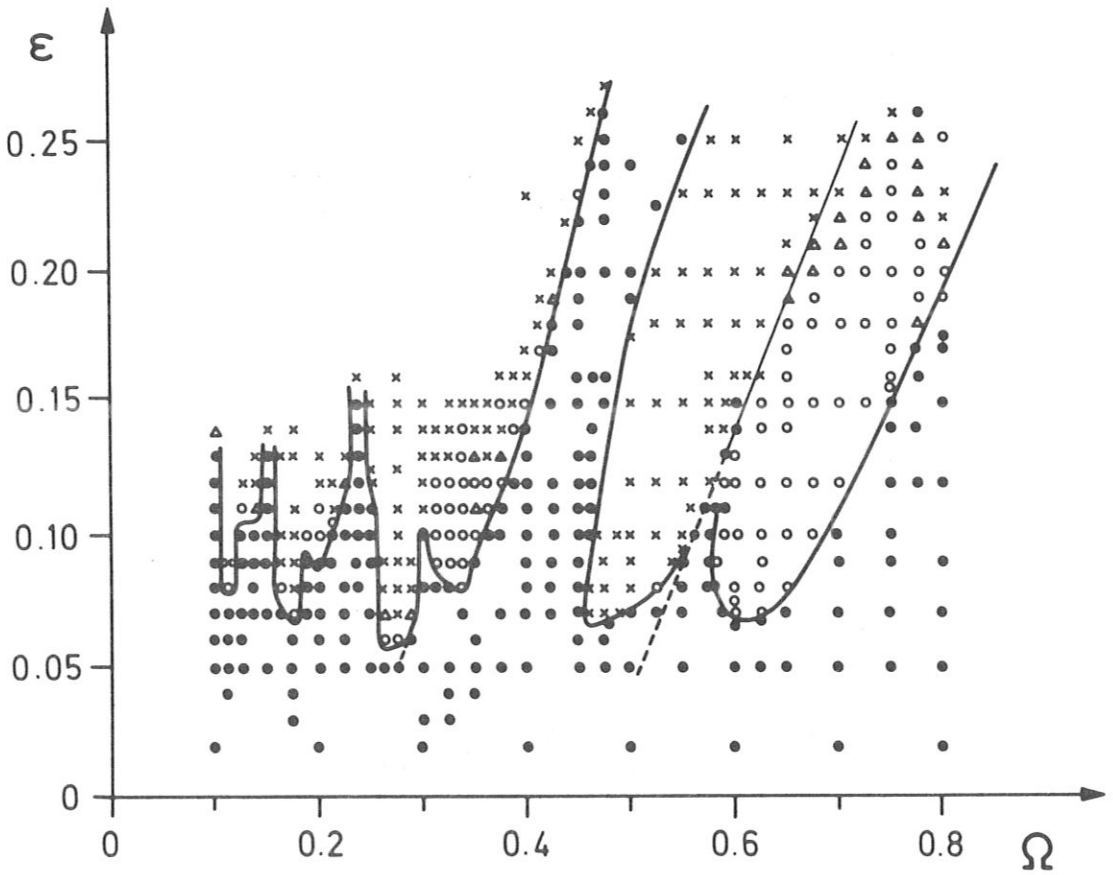

Figure 5

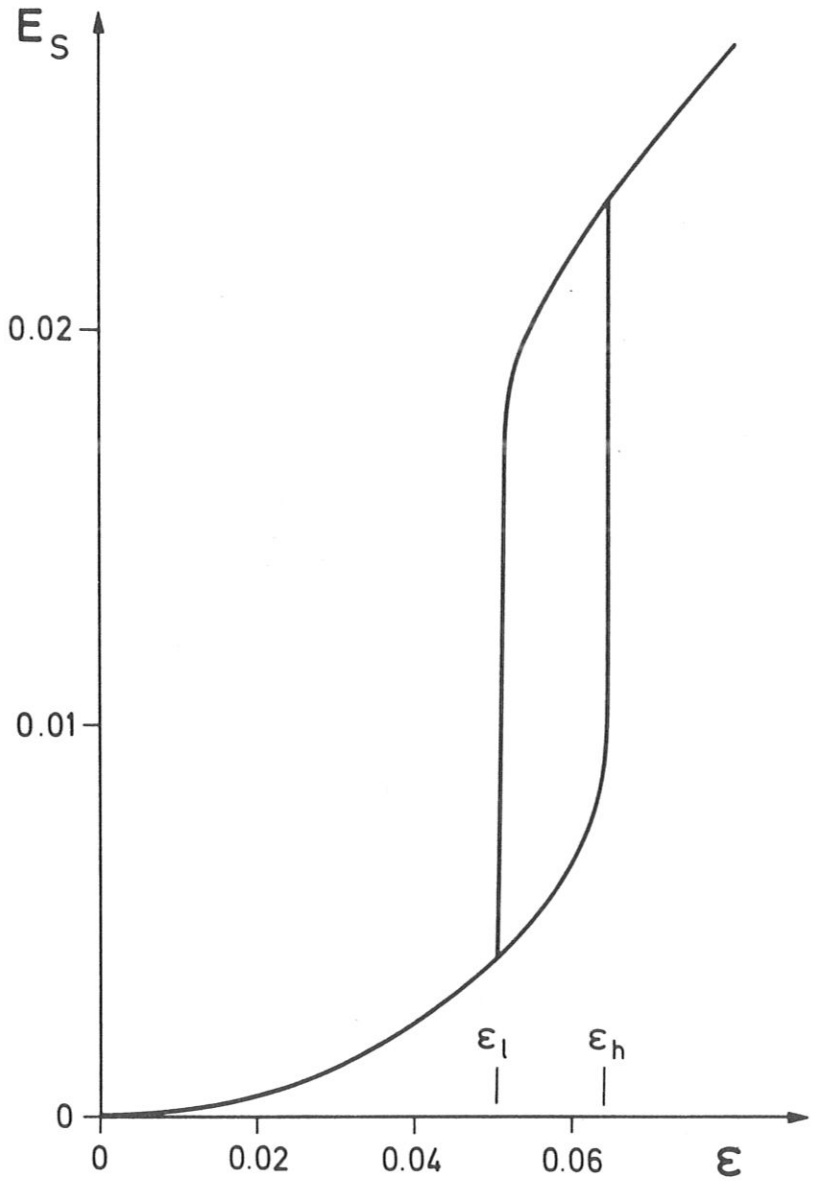
E_S
0.02
0.01
0
0
0.02
0.04
0.06
ε
ε_l
ε_h

Figure 6

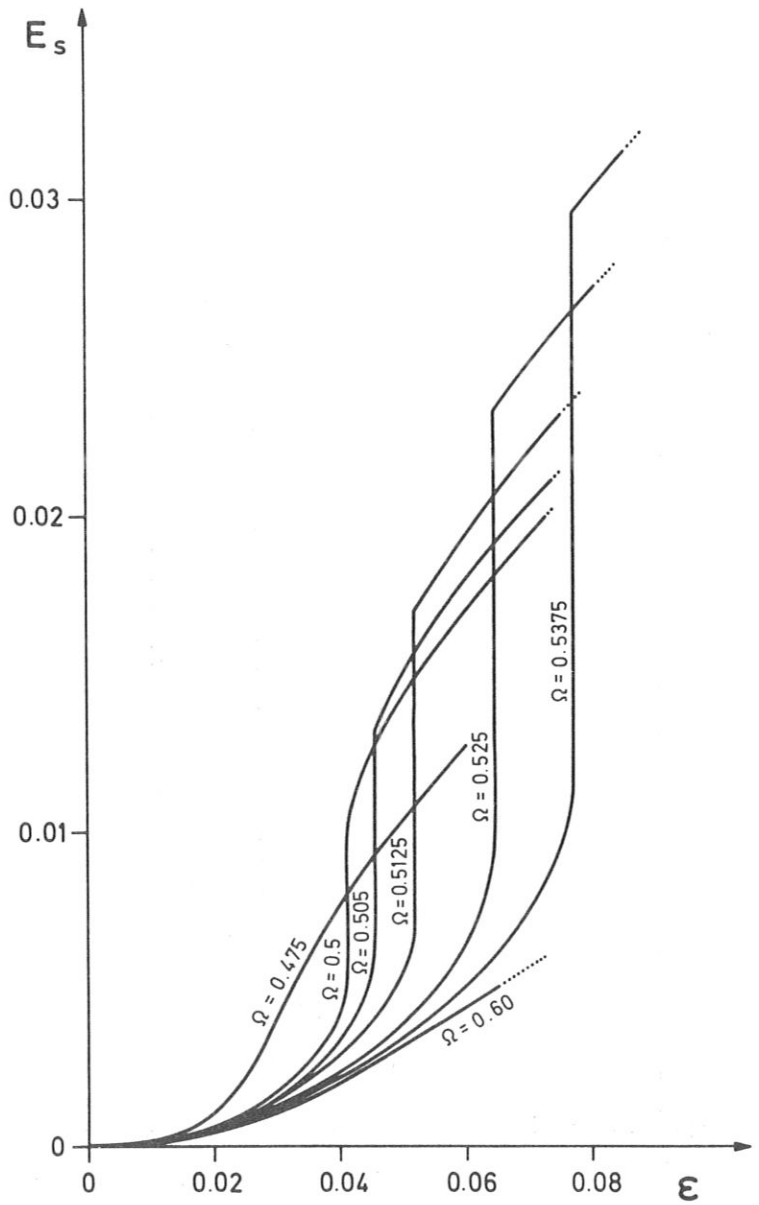
E_s
0.03
0.02
0.01
0
0
0.02
0.04
0.06
0.08
ε
$\Omega = 0.475$
$\Omega = 0.5$
$\Omega = 0.505$
$\Omega = 0.5125$
$\Omega = 0.525$
$\Omega = 0.5375$
$\Omega = 0.60$

Figure 7

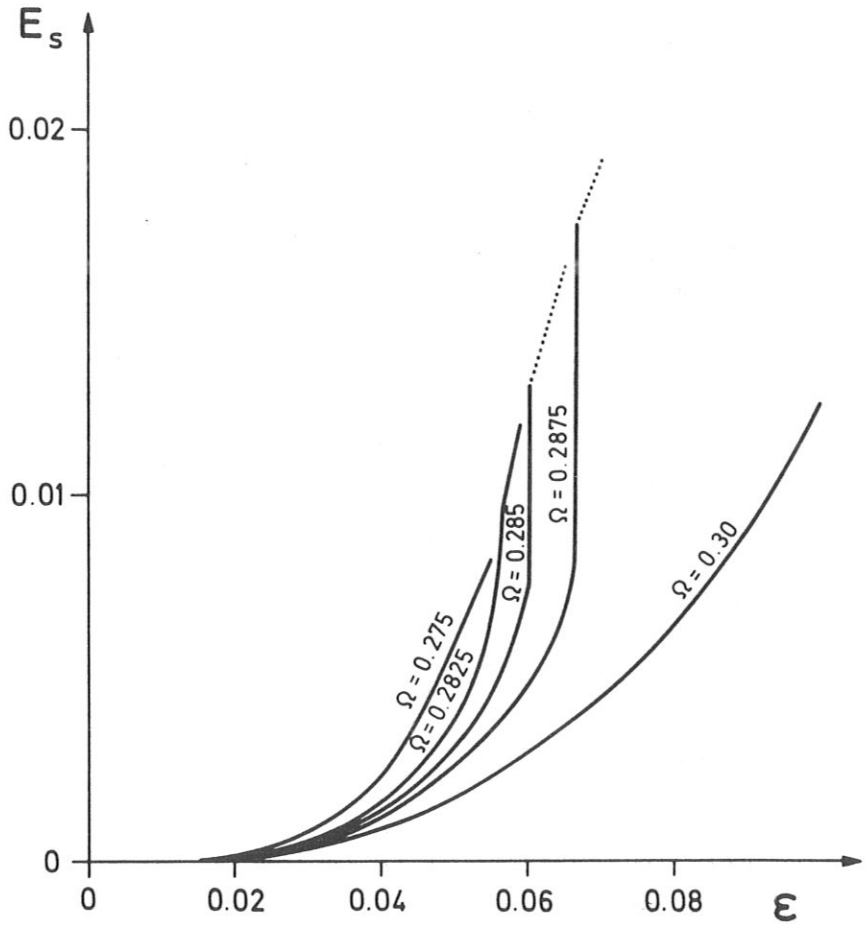
E_s
0.02
0.01
0
0
0.02
0.04
0.06
0.08
ε
$\Omega = 0.275$
$\Omega = 0.2825$
$\Omega = 0.285$
$\Omega = 0.2875$
$\Omega = 0.30$

Figure 8

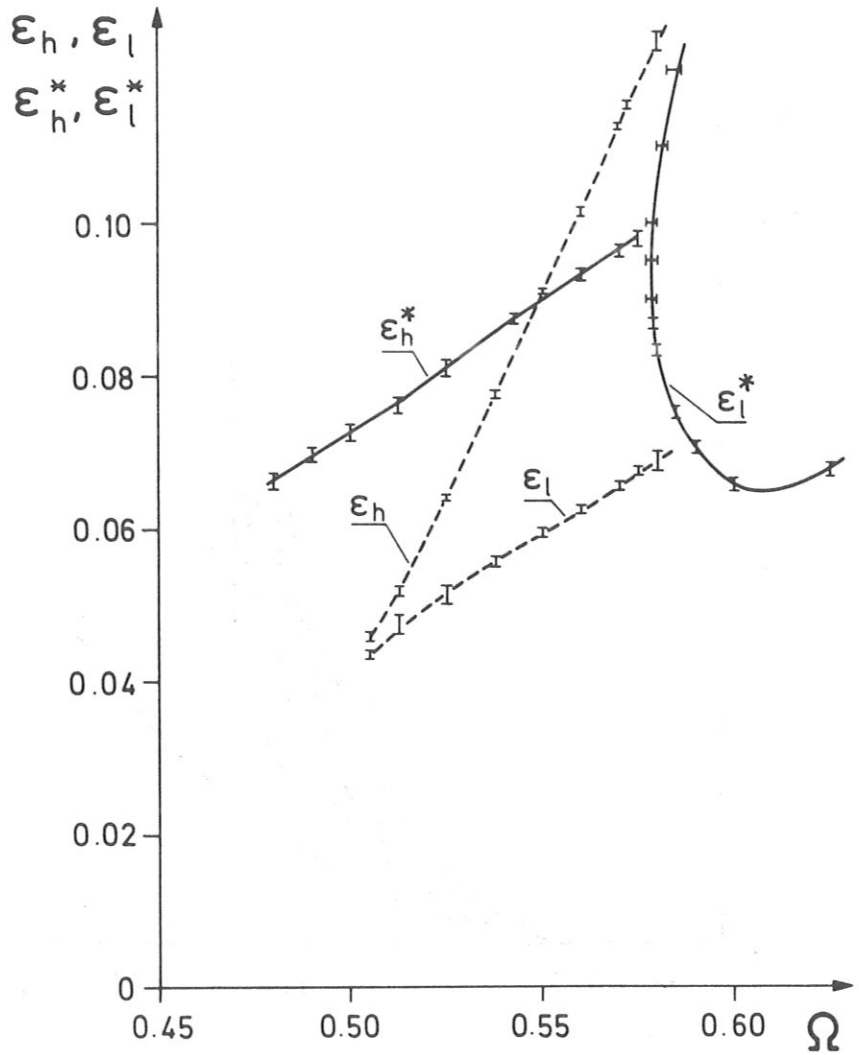
$\varepsilon_h, \varepsilon_l$
$\varepsilon_h^*, \varepsilon_l^*$
0.10
0.08
0.06
0.04
0.02
0
0.45
0.50
0.55
0.60
Ω
ε_h^*
ε_l^*
ε_l
ε_h

Figure 9

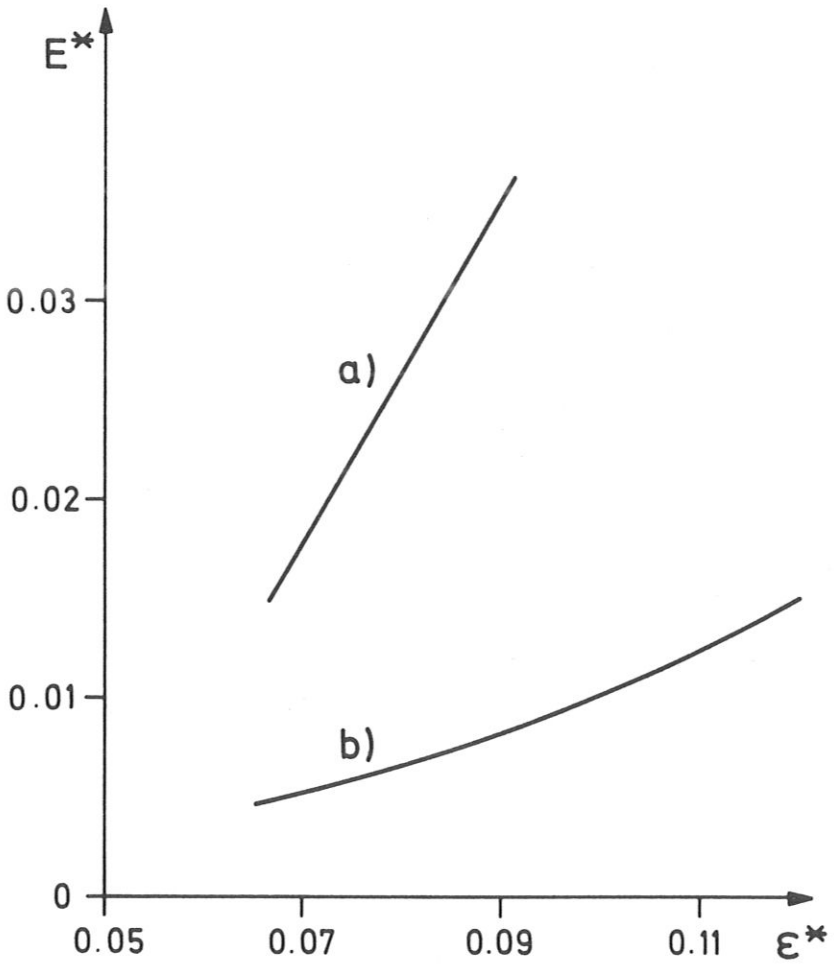

Figure 10

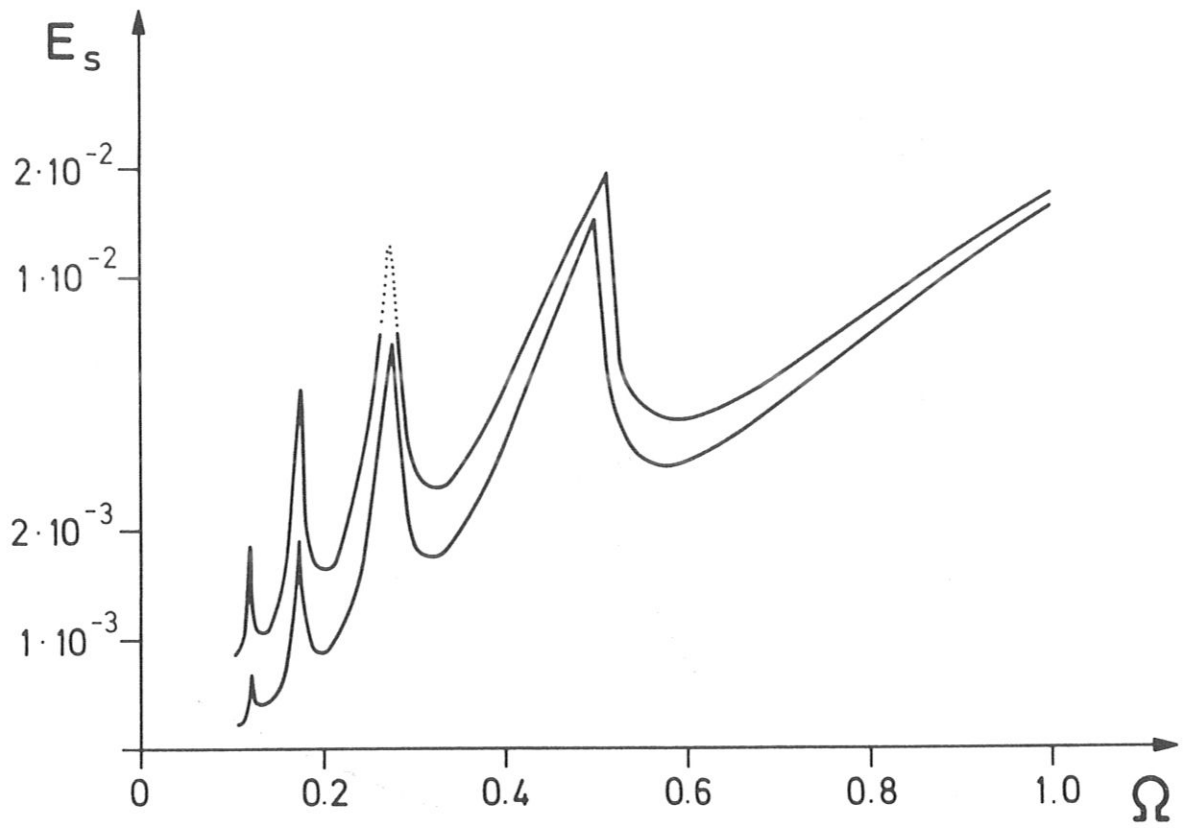

Figure 11

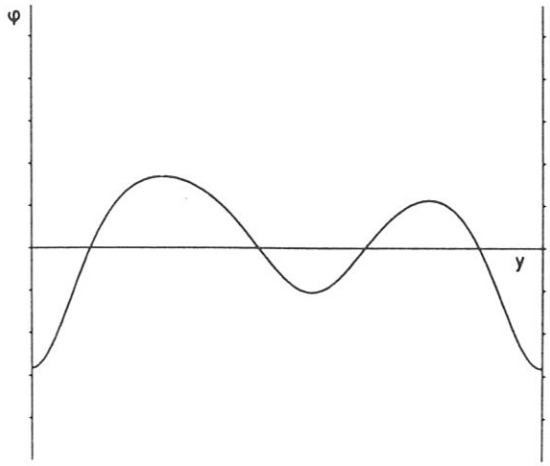

Figure 12a

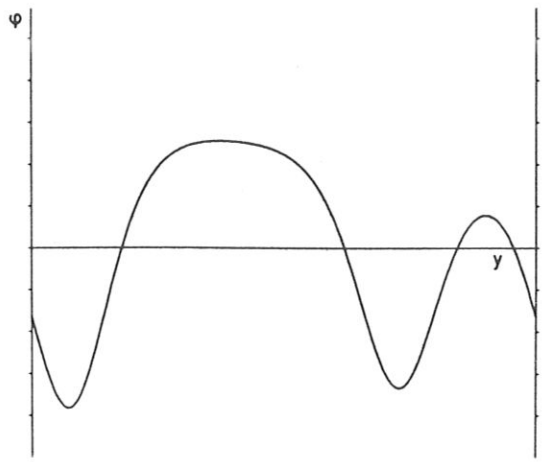

Figure 12b

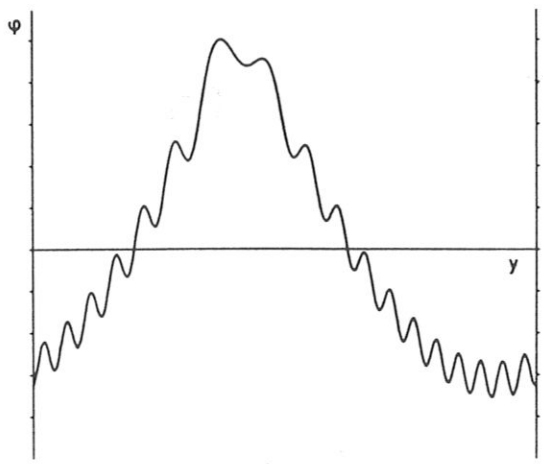

Figure 13

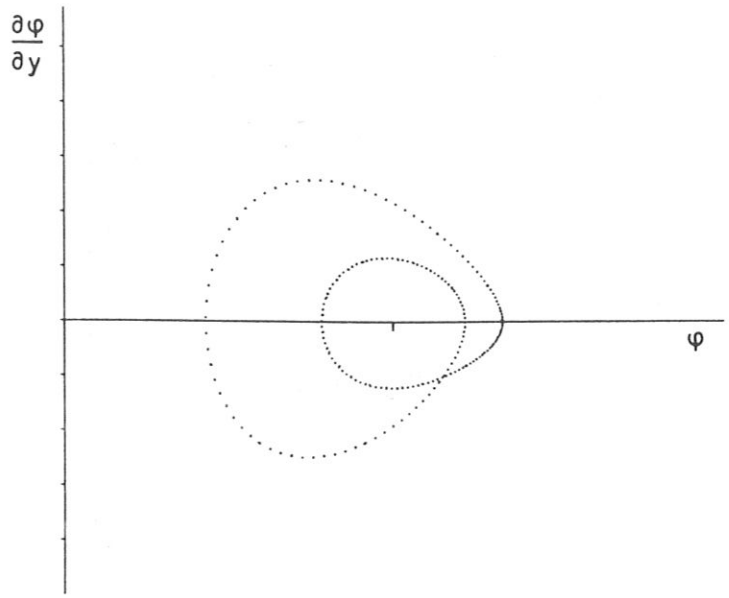

Figure 14a

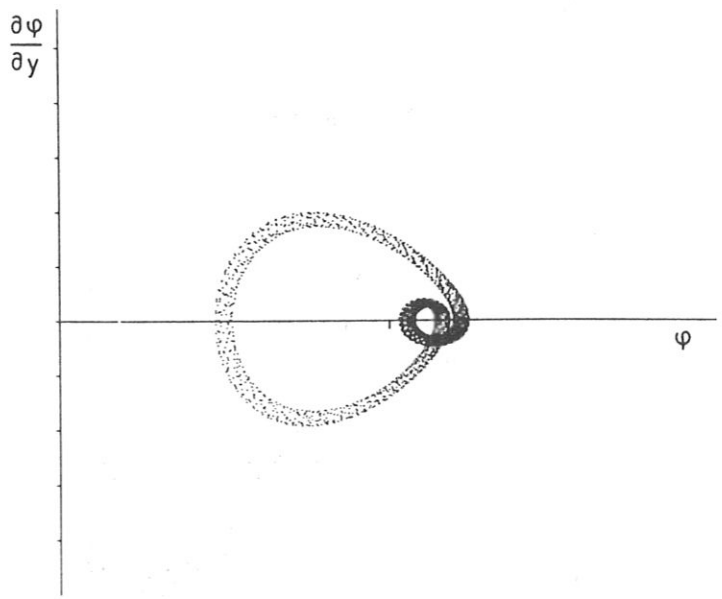

Figure 14b

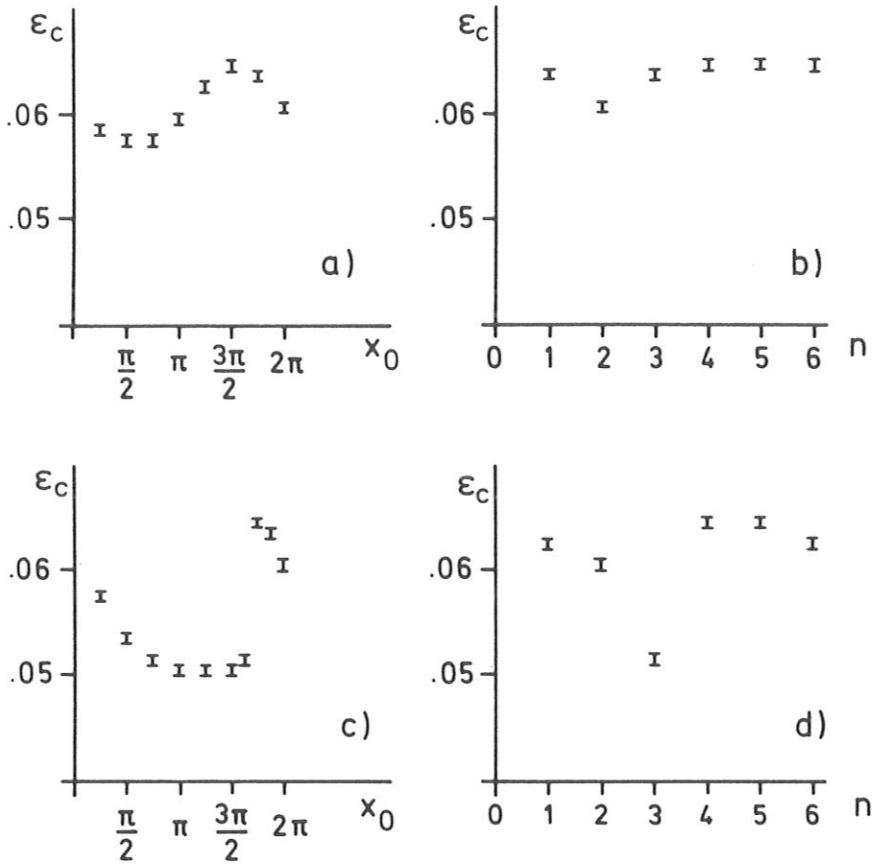

Figure 15